

RELATIVISTIC WIND BUBBLES AND AFTERGLOW SIGNATURES

Z. G. DAI

Department of Astronomy, Nanjing University, Nanjing 210093, China; dzg@nju.edu.cn

Draft version August 20, 2018

ABSTRACT

Highly magnetized, rapidly rotating compact objects are widely argued as central energy sources of γ -ray bursts (GRBs). After the GRB, such a magnetar-like object may directly lose its rotational energy through some magnetically-driven processes, which produce an ultrarelativistic wind dominated possibly by the energy flux of electron-positron pairs. The interaction of such a wind with an outward-expanding fireball leads to a relativistic wind bubble, being regarded as a relativistic version of the well-studied Crab Nebula. We here explore the dynamics of this wind bubble and its emission signatures. We find that when the injection energy significantly exceeds the initial energy of the fireball, the bulk Lorentz factor of the wind bubble decays more slowly than before, and more importantly, the reverse-shock emission could dominate the afterglow emission, which yields a bump in afterglow light curves. In addition, high polarization of the bump emission would be expected if a toroidal magnetic field in the shocked wind dominates over the random component.

Subject headings: gamma-rays: bursts — relativity — shock waves — stars: winds, outflows

1. INTRODUCTION

The recent observation of high linear polarization during the prompt γ -ray emission of GRB 021206 (Coburn & Boggs 2003) suggests that GRBs be driven by highly magnetized, rapidly rotating compact objects. Two popular scenarios for their birth are the merger of a compact binary or the collapse of a massive star (for a recent review see Mészáros 2002). In both scenarios, a rapidly rotating black hole surrounded by an accretion disk seems to be a common remnant (Narayan, Paczyński & Piran 1992; Woosley 1993; Mészáros & Rees 1997a; Paczyński 1998). However, a millisecond magnetar has also been argued as an alternative interesting product (Usov 1992; Duncan & Thompson 1992; Kluźniak & Ruderman 1998; Dai & Lu 1998; Spruit 1999; Ruderman, Tao & Kluźniak 2000; Wheeler et al. 2000). To explain the complex temporal feature, the burst itself, in some of these energy models, is understood to arise from a series of explosive reconnection events in a rising, amplified magnetic field because of the Parker instability. This in fact dissipates the differentially rotational energy and magnetic energy of the newborn magnetar or accretion disk.

After the GRB, the remaining object is reasonably assumed to be a millisecond magnetar or a rapidly rotating black hole surrounded by an accretion disk. For the latter object, the magnetic field in the disk could have been amplified initially by differential rotation to a magnetar-like strength of $\sim 10^{15}$ G, and particularly, within the framework of the collapsar/hypernova model, such a field could be kept, due to longevity (with days or longer) of the disk maintained by fallback of the ejecta. During the afterglow, the object at the center will directly lose its rotational energy by the magnetic dipole radiation or the Blandford-Znajek mechanism.

An energy outflow driven magnetically includes three components: low-frequency electromagnetic waves, a relativistic wind, and a toroidal magnetic field associated with the wind. The wind energy flux is unlikely to be baryon-

dominated, because the initial explosion should have left a clean passage with very few baryon contamination for a subsequent outflow. The interaction of this outflow with an outward-expanding fireball implies a continuous injection of the stellar rotational energy into the fireball. Dai & Lu (1998, 2000), Zhang & Mészáros (2001) and Chang, Lee & Yi (2002) discussed the evolution of a relativistic fireball by assuming a pure electromagnetic-wave energy outflow, while Rees & Mészáros (1998), Sari & Mészáros (2000), Zhang & Mészáros (2002), and Granot, Nakar & Piran (2003) took into account a variable and baryon-dominated injection.

However, based on the successful models of the well-observed Crab Nebula (Rees & Gunn 1974; Kennel & Coroniti 1984; Begelman & Li 1992; Chevalier 2000), a realistic, continuous outflow during the afterglow is expected to be ultra-relativistic and dominated by the energy flux of electron-positron pairs. As in the Crab Nebula, even if an outflow from the pulsar is Poynting-flux-dominated at small radii, the fluctuating component of the magnetic field in this outflow can be dissipated by magnetic reconnection and used to accelerate the outflow, which is eventually dominated by the energy flux of e^+e^- pairs within a larger radius $\sim 10^{17}$ cm (Coroniti 1990; Michel 1994; Kirk & Skjæraasen 2003). In the case of an afterglow, therefore, it is natural to expect that the central object still produces an ultra-relativistic e^+e^- -pair wind, whose interaction with the fireball leads to a relativistic wind bubble. This can be regarded as a *relativistic version of the Crab Nebula*.

In this paper, we explore the dynamics of such a wind bubble and its emission signatures. In §2 we present expressions of the luminosity of a relativistic wind from a highly magnetized, rapidly rotating object. In §§3 and 4 we discuss evolution of the wind bubble and temporal features of the radiation respectively. In the final section we summarize our findings and give a brief discussion on implications of the bubble.

2. THE LUMINOSITY OF A RELATIVISTIC WIND

We assume that a burst itself arises from a series of explosive reconnection events. After the GRB, we are left with a highly magnetized, rapidly rotating compact object. Let's first assume that it is a millisecond magnetar with period P , surface magnetic field strength B_s , moment of inertia I , radius R_M , and angle between the rotation axis and magnetic dipole moment θ . Since such a pulsar loses its rotational energy through the magnetic dipole torque, the luminosity of a resulting relativistic wind is given by

$$L_w \simeq 4 \times 10^{47} B_{\perp,14}^2 R_{M,6}^6 P_{\text{ms}}^{-4} \text{ erg s}^{-1}, \quad (1)$$

where $B_{\perp,14} = B_s \sin \theta / 10^{14} \text{ G}$, $R_{M,6} = R_M / 10^6 \text{ cm}$, and $P_{\text{ms}} = P / 1 \text{ ms}$. Because of spin-down, this luminosity will evolve with time as

$$L_w \propto (1 + t/T_{M,0})^{-2} \begin{cases} \sim \text{const.}, & \text{if } t < T_{M,0}, \\ \propto t^{-2}, & \text{if } t > T_{M,0}, \end{cases} \quad (2)$$

where t is the observer time in units of day, $T_{M,0} = 0.58 B_{\perp,14}^{-2} I_{45} R_{M,6}^{-6} P_{0,\text{ms}}^2$ days is the “initial” spin-down timescale of the magnetar at the onset of the afterglow, $P_0 = P_{0,\text{ms}} \times 1 \text{ ms}$ is the rotation period at this time, and $I_{45} = I / 10^{45} \text{ g cm}^2$. Usov (1992) also assumed that the early spin-down could be due to gravitational wave radiation besides magnetic dipole radiation. However, the luminosity for gravitational wave radiation depends on the stellar ellipticity which is poorly known, and so we neglected the effect of this mechanism on spin-down.

We now discuss another case in which the central object is a rapidly rotating black hole surrounded by an accretion disk. If the amplified magnetic field in the disk does not evolve significantly with time during fallback of the ejecta, the rotational energy of this black hole will be gradually extracted by the Blandford-Znajek mechanism, whose luminosity is approximated by

$$L_w = 1.5 \times 10^{51} B_{\text{BH},15}^2 (M_{\text{BH}}/3M_{\odot})^2 a^2 f(a) \text{ erg s}^{-1} \simeq 3 \times 10^{47} B_{\text{BH},15}^2 (M_{\text{BH}}/3M_{\odot})^2 (a/0.2)^4 \text{ erg s}^{-1}, \quad (3)$$

where $f(a) = 1 - [(1 + \sqrt{1 - a^2})/2]^{1/2} \simeq a^2/8$ for the rotation parameter $a \ll 1$, M_{BH} is the black-hole mass, and $B_{\text{BH},15}$ is the disk field strength in units of 10^{15} G (Lee, Wijers & Brown 2000). We note that a typical value ($\sim 10^{47} \text{ erg s}^{-1}$) of the wind luminosity in equations (1) and (3) has been invoked by Rees & Mészáros (2000) to explain the observed iron lines from some GRBs within the framework of the collapsar/hypernova model. Considering the rotational energy of the black hole $E_{\text{BH}} = f(a)M_{\text{BH}}c^2 \simeq (a^2/8)M_{\text{BH}}c^2$ for $a \ll 1$ (Lee et al. 2000), and assuming $\dot{E}_{\text{BH}} = L_w$, we find that the Blandford-Znajek mechanism yields spin-down, similarly to the magnetar case, if the accreted angular momentum is neglected because its rate seems to be below the torque driven by the Blandford-Znajek mechanism at time of days after the burst for typical parameters in the collapsar/hypernova model. Thus, we obtain a crude evolution law of the above luminosity,

$$L_w \propto (1 + t/T_{\text{BH},0})^{-2} \begin{cases} \sim \text{const.}, & \text{if } t < T_{\text{BH},0}, \\ \propto t^{-2}, & \text{if } t > T_{\text{BH},0}, \end{cases} \quad (4)$$

where $T_{\text{BH},0} = 1.0 B_{\text{BH},15}^{-2} (M_{\text{BH}}/3M_{\odot})^{-1} (a_0/0.2)^{-2}$ days is the “initial” spin-down time of the black hole and a_0 is the “initial” rotation parameter. One can easily see that equations (2) and (4) are similar, which implies that our discussion of a relativistic wind bubble in the remaining text for magnetars should be valid for black holes.

3. THE BUBBLE DYNAMICS IN THE THIN-SHELL APPROXIMATION

Similarly to the Crab Nebula, a rotating magnetar at the center of an afterglow generates a highly relativistic wind dominated by the energy flux of e^+e^- pairs, with bulk Lorentz factor of $\gamma_w \sim 10^4 - 10^7$. Atoyan (1999) argued that the Crab pulsar initially had $\gamma_w \sim 10^4$ to interpret the measured radio spectrum of the Crab Nebula. We adopt $\gamma_w = 10^4$ as a fiducial value in our calculations. Because γ_w is much larger than the Lorentz factor of the medium swept up by the fireball, this wind passes through a shock front and decelerates to match the expansion velocity of the swept-up medium. Therefore, a relativistic wind bubble, as a result of interaction of the wind with the medium, should include two shocks: a reverse shock that propagates into the cold wind and a forward shock that propagates into the ambient medium. Thus, there are four regions separated in the bubble by these shocks: (1) the unshocked medium, (2) the forward-shocked medium, (3) the reverse-shocked wind gas, and (4) the unshocked cold wind, where regions 2 and 3 are separated by a contact discontinuity. For simplicity, we here assume that two initially-forming forward shocks during interactions of the fireball both with the medium and with the wind have eventually merged to one forward shock, and also neglect effects of the baryon loading whose mass is much less than the swept-up mass, when the observer time far exceeds the initial deceleration timescale.

We denote n_i and P'_i as the baryon number density and pressure of region “ i ” in its own rest frame respectively, and γ_i is the Lorentz factor of region “ i ” measured in the local medium’s rest frame. We derive the relative Lorentz factor of region 3 measured in the rest frame of region 4 as $\gamma_{34} \simeq (1/2)(\gamma_w/\gamma_3 + \gamma_3/\gamma_w) \simeq \gamma_w/(2\gamma_3) \gg 1$ for $\gamma_w \gg \gamma_3 \gg 1$, implying a relativistic reverse shock. Because the electron number density in the rest frame comoving with the unshocked wind is $n_4 = L_w/(4\pi r^2 \gamma_w^2 m_e c^3)$ (where r is the radius of region 3 and m_e is the electron mass), according to the jump conditions for a relativistic shock (Blandford & McKee 1976), the pressure of region 3 is calculated by

$$P'_3 = \frac{4}{3} \gamma_{34}^2 n_4 m_e c^2 \simeq \frac{L_w}{12\pi r^2 \gamma_3^2}. \quad (5)$$

Neglecting the presence of the reverse shock and the radiative energy loss of region 2, and assuming an ambient interstellar medium with constant density of n_1 , the properties of the shocked medium in region 2 should satisfy the Blandford-McKee adiabatic self-similarity solution with the similarity variable at any radius r ,

$$\chi = (1 + 16\gamma_2^2) \left(1 - \frac{r}{ct_1} \right), \quad (6)$$

where $\gamma_2 \equiv \gamma_2(R)$ is the Lorentz factor of the shocked medium just behind the forward shock whose radius is

denoted as R , and $t_l = (R/c)[1 + 1/(16\gamma_2^2)]$ is the time measured in the local medium's rest frame. The radius r can thus be expressed as function of χ by

$$r = R \left(1 + \frac{1}{16\gamma_2^2}\right) \left(1 - \frac{\chi}{1 + 16\gamma_2^2}\right), \quad (7)$$

which implies $r \simeq R$ as long as $\chi \ll 16\gamma_2^2$ for an ultrarelativistic forward shock. This justifies the *thin-shell approximation*, in which the width of region 2 is insignificant as compared to the shock radius R .

According to Blandford & McKee (1976), the pressure and Lorentz factor of the shocked medium at radius r are given by

$$P'_2(r) = \frac{4}{3}n_1m_p c^2 \gamma_2^2 \chi^{-17/12}, \quad (8)$$

$$\gamma_2(r) = \gamma_2 \chi^{-1/2}, \quad (9)$$

where m_p is the proton mass. Along the contact discontinuity, $\gamma_3 = \gamma_2(r)$ and $P'_3 = P'_2(r)$, which yield

$$\gamma_3 = \gamma_2 \chi^{-1/2}, \quad (10)$$

$$\chi^{-17/12} = \frac{L_w}{16\pi n_1 m_p c^3 \gamma_2^2 \gamma_3^2 R^2}, \quad (11)$$

where the thin-shell approximation $r \simeq R$ has been considered. For an ultrarelativistic, adiabatic forward shock, Blandford & McKee (1976) found its total energy,

$$E_0 = \frac{16\pi n_1 m_p c^2 \gamma_2^2 R^3}{17}. \quad (12)$$

In deriving the temporal laws of the similarity variable at the location of the contact discontinuity and the Lorentz factors of regions 2 and 3, we should note one crucial effect that the photons that are radiated from regions 2 and 3 at the same time in the local medium's rest frame will be detected at different observer times. This is because the Lorentz factor of region 3 is smaller than $\gamma_2(R)$ by a factor of $\chi^{-1/2}$ so that for a same time interval in the local medium's rest frame, R/c , the emission from region 3 will reach the observer at time,

$$t \simeq \frac{R}{4\gamma_3^2 c}, \quad (13)$$

and the emission from region 2 will reach the observer at time,

$$t \simeq \frac{R}{4\gamma_2^2 c}. \quad (14)$$

Using equations (12) and (14), the Lorentz factor of the shocked medium (i.e., region 2) just behind the forward shock is found to evolve with time as

$$\gamma_2 = \left(\frac{17E_0}{1024\pi n_1 m_p c^5 t^3} \right)^{1/8}. \quad (15)$$

From equations (10)-(13), we have the similarity variable at the location of the contact discontinuity,

$$\chi = \left(\frac{4L_w t}{17E_0} \right)^{-12/17} = 3.1 \left(\frac{L_{w,47} t}{E_{52}} \right)^{-12/17}, \quad (16)$$

and the Lorentz factor of region 3,

$$\begin{aligned} \gamma_3 &= \left[\frac{(4L_w)^{12/17} (17E_0)^{5/17}}{1024\pi n_1 m_p c^5 t^{39/17}} \right]^{1/8} \\ &= 5.3 L_{w,47}^{3/34} E_{52}^{5/136} n_1^{-1/8} t^{-39/136} \end{aligned} \quad (17)$$

where $L_{w,47} = L_w/10^{47}$ erg s⁻¹, $E_{52} = E_0/10^{52}$ ergs, and n_1 and t are in units of 1 cm⁻³ and 1 day respectively.

Letting $\chi = 1$, we define a critical time

$$t_{\text{cr}} = 4.9 E_{52} L_{w,47}^{-1} \text{ days}. \quad (18)$$

At this time, the injection energy to the fireball significantly exceeds its initial energy. For $t < t_{\text{cr}}$, the similarity variable $\chi > 1$. It should be emphasized that the dynamics denoted by equation (17) is simply calculated by equating the pressures of the two-sided shocked fluids at the contact discontinuity. In this derivation, we have neglected any work done on region 2 by region 3 because the pressure of region 3 is much less than $P'_2(R)$ at $t < t_{\text{cr}}$.

Once the observer's time exceeds t_{cr} , the similarity variable $\chi = 1$. At this stage, the total kinetic energy of region 2 is approximated as $E_{\text{kin},2} = (\gamma_2^2 - 1)M_{\text{sw}}c^2$, where $M_{\text{sw}} = (4\pi/3)R^3 n_1 m_p$ is the swept-up medium mass. Energy conservation requires that any increase of kinetic energy of region 2 should be equal to work done by region 3,

$$dE_{\text{kin},2} = \gamma_3 P'_3 dV'_3, \quad (19)$$

where $dV'_3 = 4\pi R^2 dR' = 4\pi R^2 (dR/\gamma_3)$ is the volume change of region 3 in its own rest frame. Since regions 2 and 3 should keep velocity equality along the contact discontinuity (viz., $\gamma_2 = \gamma_3$), we rewrite equation (19) as

$$\frac{d\gamma_2}{dR} = \frac{4\pi R^2 [P'_3 - (\gamma_2^2 - 1)n_1 m_p c^2]}{2\gamma_2 M_{\text{sw}} c^2}. \quad (20)$$

Considering equation (5) and the shock radius $R \simeq 4\gamma_2^2 ct$, the solution of equation (20) becomes

$$\gamma_2 = \gamma_3 = \left(\frac{L_w}{128\pi n_1 m_p c^5 t^2} \right)^{1/8}, \quad (21)$$

where the dependence of γ_2 on t is consistent with the one derived for a pure electromagnetic energy injection by Dai & Lu (1998).

We next discuss the dynamics of a relativistic wind bubble: In the case of $t_{\text{cr}} > T_{\text{M},0}$ (viz., $E_{52} > 0.46 I_{45} P_{0,\text{ms}}^{-2}$), the wind bubble should evolve based on equations (15) and (17); for $t_{\text{cr}} < T_{\text{M},0}$ (viz., $E_{52} < 0.46 I_{45} P_{0,\text{ms}}^{-2}$), however, the Lorentz factors of the wind bubble decay initially as $\gamma_2 \propto t^{-3/8}$ and $\gamma_3 \propto t^{-39/136}$ at $t < t_{\text{cr}}$ (stage I), subsequently as $\gamma_2 = \gamma_3 \propto t^{-1/4}$ at $t \in (t_{\text{cr}}, T_{\text{M},0})$ (stage II), and finally again as $\gamma_2 \propto t^{-3/8}$ at $t > T_{\text{M},0}$ (stage III). It should be pointed out that this discussion assumes a negligible radiative loss of region 3. However, no matter whether region 3 is at stage I or II, and once it enters the fast cooling regime at some time, its pressure will begin to become much smaller than that of region 2 and then the Lorentz factor of region 2 will decay as equation (15).

4. SYNCHROTRON RADIATION AND LIGHT CURVES

In this section we discuss light curves of the emission from a relativistic wind bubble, assuming $t_{\text{cr}} < T_{M,0}$. The dynamics above determines the bulk Lorentz factor and the thermal Lorentz factors of the accelerated electrons of each region as function of time. We consider synchrotron radiation from each region at different stages. According to the standard afterglow model (Mészáros & Rees 1997b; Sari, Piran & Narayan 1998), the spectrum consists of four power-law segments separated by three break frequencies: the self-absorption frequency ν_a , the characteristic frequency ν_m , and the cooling frequency ν_c , with the peak flux $F_{\nu,\text{max}}$. To calculate them, we assume that for region 3 the electron and magnetic field energy densities are fractions ϵ_e and ϵ_B of the total energy density behind the reverse shock (where $\epsilon_e + \epsilon_B = 1$), but for region 2, fractions ξ_e and ξ_B of the total energy density behind the forward shock (where $\xi_e + \xi_B < 1$). One may expect that $\epsilon_e \neq \xi_e$ and/or $\epsilon_B \neq \xi_B$, as suggested in some recent studies (Coburn & Boggs 2003; Zhang, Kobayashi & Mészáros 2003; Kumar & Panaiteescu 2003). In addition, we assume that the spectral index of the electron energy distribution is p for region 3 and q for region 2.

At stage I ($t < t_{\text{cr}}$), the break frequencies and peak flux of region 3 are derived as

$$\begin{aligned} \nu_{m,3}^{\text{I}} &= 6.8 \times 10^{12} g_p^2 \epsilon_e^2 \epsilon_{B,-1}^{1/2} \gamma_{w,4}^2 \\ &\times L_{w,47}^{5/34} E_{52}^{-5/34} n_1^{1/2} t^{5/34} \text{ Hz}, \end{aligned} \quad (22)$$

$$\begin{aligned} \nu_{c,3}^{\text{I}} &= 3.0 \times 10^{14} \epsilon_{B,-1}^{-3/2} L_{w,47}^{-27/34} \\ &\times E_{52}^{5/17} n_1^{-1} t^{-22/17} \text{ Hz}, \end{aligned} \quad (23)$$

$$\begin{aligned} F_{\nu,\text{max},3}^{\text{I}} &= 88 \epsilon_{B,-1}^{1/2} \gamma_{w,4}^{-1} L_{w,47}^{45/34} E_{52}^{-5/68} \\ &\times n_1^{1/4} D_{L,28}^{-2} t^{39/68} \text{ mJy}, \end{aligned} \quad (24)$$

where $g_p = (p-2)/(p-1)$, $\epsilon_{B,-1} = \epsilon_B/0.1$, $\gamma_{w,4} = \gamma_w/10^4$, and $D_{L,28}$ is the luminosity distance to the source in units of 10^{28} cm. We here considered only the characteristic frequency and the cooling frequency for the optical to X-ray emission discussed in this paper. In our derivation, we used equations (8), (10) and (17) to obtain the energy density of region 3, $e'_3 = 4n_1 m_p c^2 \gamma_2^2 \chi^{-17/12} = 4n_1 m_p c^2 \gamma_3^2 \chi^{-5/12} = 0.11 L_{w,47}^{8/17} E_{52}^{-15/68} n_1^{3/4} t^{-19/68} \text{ erg cm}^{-3}$, and the magnetic field strength, $B'_3 = (8\pi \epsilon_B e'_3)^{1/2} = 0.52 \epsilon_{B,-1}^{1/2} L_{w,47}^{4/17} E_{52}^{-15/136} n_1^{3/8} t^{-19/136} \text{ G}$. We define a cooling time $t_{0,3}^{\text{I}}$ through $\nu_{m,3}^{\text{I}} = \nu_{c,3}^{\text{I}}$ as

$$\begin{aligned} t_{0,3}^{\text{I}} &= 14(g_p \epsilon_e \epsilon_{B,-1} \gamma_{w,4})^{-68/49} \\ &\times L_{w,47}^{-32/49} E_{52}^{15/49} n_1^{-51/49} \text{ days}. \end{aligned} \quad (25)$$

From equations (22) and (23), we find that region 3 is in the slow-cooling regime for $t < t_{0,3}^{\text{I}}$ but in the fast-cooling regime for $t > t_{0,3}^{\text{I}}$, in contrast to the standard afterglow model (Sari et al. 1998). A larger value of γ_w would imply fast cooling in region 3 earlier on, in which case region 2 could still stay at stage I. For region 2, the break frequencies and peak flux are given by

$$\nu_{m,2}^{\text{I}} = 1.6 \times 10^{13} g_q^2 \xi_{e,-1}^2 \xi_{B,-1}^{1/2} E_{52}^{1/2} t^{-3/2} \text{ Hz}, \quad (26)$$

$$\nu_{c,2}^{\text{I}} = 8.5 \times 10^{13} \xi_{B,-1}^{-3/2} E_{52}^{-1/2} n_1^{-1} t^{-1/2} \text{ Hz}, \quad (27)$$

$$F_{\nu,\text{max},2}^{\text{I}} = 35 \xi_{B,-1}^{1/2} E_{52} n_1^{1/2} D_{L,28}^{-2} \text{ mJy}, \quad (28)$$

where $g_q = (q-2)/(q-1)$, $\xi_{e,-1} = \xi_e/0.1$, and $\xi_{B,-1} = \xi_B/0.1$ (Sari et al. 1998).

At stage II ($t_{\text{cr}} < t < T_{M,0}$), since $\gamma_2 \propto t^{-1/4}$, we obtain the break frequencies and the peak flux for region 3,

$$\nu_{m,3}^{\text{II}} \propto t^0, \quad \nu_{c,3}^{\text{II}} \propto t^{-1}, \quad F_{\nu,\text{max},3}^{\text{II}} \propto t^{1/2}, \quad (29)$$

and for region 2,

$$\nu_{m,2}^{\text{II}} \propto t^{-1}, \quad \nu_{c,2}^{\text{II}} \propto t^{-1}, \quad F_{\nu,\text{max},2}^{\text{II}} \propto t^1. \quad (30)$$

We define another cooling time $t_{0,3}^{\text{II}}$ at which $\nu_{m,3}^{\text{II}} = \nu_{c,3}^{\text{II}}$ as follows

$$t_{0,3}^{\text{II}} = 22(g_p \epsilon_e \epsilon_{B,-1} \gamma_{w,4})^{-2} L_{w,47}^{-1/2} n_1^{-3/2} \text{ days}. \quad (31)$$

Equation (29) is valid only for $t < \min(t_{0,3}^{\text{II}}, T_{M,0})$. Otherwise, once region 3 enters the fast-cooling regime or the wind luminosity weakens obviously, its pressure becomes insignificant as compared to that of region 2 and thus evolution of the wind bubble comes back to $\gamma_2 \propto t^{-3/8}$.

We assume $t_{0,3}^{\text{II}} < T_{M,0}$. If $t_{\text{cr}} < t < t_{0,3}^{\text{II}}$, then region 3 is adiabatic and its emission spectrum is determined by equation (29). If $t_{0,3}^{\text{II}} < t < T_{M,0}$, region 3 becomes fast cooling, and the break frequencies and the peak flux for region 2 evolve as $\nu_{m,2}^{\text{II}} \propto t^{-3/2}$, $\nu_{c,2}^{\text{II}} \propto t^{-1/2}$ and $F_{\nu,\text{max},2}^{\text{II}} \propto t^0$. At stage III, the emission flux of region 3: $F_{\nu,3}^{\text{III}} \propto \nu^{-\beta} t^{-(2+\beta)}$, where β is the spectral index at $t_{0,3}^{\text{II}}$ (Kumar & Panaiteescu 2000).

On the other hand, $t_{0,3}^{\text{II}} > T_{M,0}$ is assumed. If $t_{\text{cr}} < t < T_{M,0}$, the spectrum and light curves for regions 3 and 2 are obtained by using equations (29) and (30), respectively. But if $t > T_{M,0}$ (stage III), because of adiabatic expansion of region 3, the break frequencies and the peak flux decay as $\nu_{m,3}^{\text{III}} \propto t^{-73/48}$, $\nu_{c,3}^{\text{III}} \propto t^{-73/48}$ and $F_{\nu,\text{max},3}^{\text{III}} \propto t^{-47/48}$ (Sari & Piran 1999).

According to the derived scaling laws of the break frequencies and peak flux with time at three stages, we can obtain the light curve indices for different frequency bands in the case of $t_{\text{cr}} < T_{M,0}$ (see Table 1). As an example, Figure 1 presents R-band light curves for typical values of the model parameters: $I_{45} = 3$, $P_{0,\text{ms}} = 1$, $\gamma_{w,4} = 1$, $L_{w,47} = 1$, $p = q = 2.5$, $\epsilon_e = 0.9$, $\epsilon_B = \xi_e = \xi_B = 0.1$, $E_{52} = 1$, $n_1 = 1 \text{ cm}^{-3}$, and $D_{L,28} = 1$. We can see that the emission flux from region 2 decays rapidly at time $< t_{\text{cr}}$, subsequently fades more slowly at time $\in (t_{\text{cr}}, T_{M,0})$, and finally declines based on the initial evolution law (Dai & Lu 1998). More importantly, the emission from region 3 dominates the afterglow emission, which leads to a bump in the afterglow light curve.

5. DISCUSSION AND CONCLUSIONS

Based on the successful models of the Crab Nebula, we discuss the dynamics of a relativistic wind bubble and its emission signatures. Such a wind bubble is naturally expected when an ultrarelativistic e^+e^- -pair wind from a highly magnetized, rapidly rotating object at the center of

region	frequency	stage I slow cooling	stage II ($t_{\text{cr}} < t < T_{M,0}$)			stage III $t_{0,3}^{\text{II}} < T_{M,0}$	
			$t < t_{0,3}^{\text{II}} < T_{M,0}$	$t_{0,3}^{\text{II}} < t < T_{M,0}$	$t_{0,3}^{\text{II}} > T_{M,0}$	$t_{0,3}^{\text{II}} < T_{M,0}$	$t_{0,3}^{\text{II}} > T_{M,0}$
3...	$\nu < \nu_p$	$-\frac{107}{204}$	$-\frac{1}{2}$	$-\frac{17}{12}$	$-\frac{1}{2}$	$\frac{5}{p+3}$	$\frac{17}{73p+21}$
	$\nu_p < \nu < \nu_0$	$-\frac{5p+34}{68}$	$-\frac{1}{2}$	$\frac{1}{4}$	$-\frac{1}{2}$	$\frac{2}{p+4}$	$\frac{96}{p+3}$
	$\nu > \nu_0$	$-\frac{5(p-2)}{68}$	0	$-\frac{p-2}{4}$	0	$\frac{2}{p+3}$	$\frac{2}{2}$
2...	$\nu < \nu_p$	$-\frac{1}{2}$	$-\frac{4}{3}$	$-\frac{1}{2}$	$-\frac{4}{3}$	$-\frac{1}{2}$	$-\frac{1}{2}$
	$\nu_p < \nu < \nu_0$	$\frac{3(q-1)}{4}$	$\frac{q-3}{2}$	$\frac{3(q-1)}{4}$	$\frac{q-3}{2}$	$\frac{3(q-1)}{4}$	$\frac{3(q-1)}{4}$
	$\nu > \nu_0$	$\frac{3q-2}{4}$	$\frac{q-2}{2}$	$\frac{3q-2}{4}$	$\frac{q-2}{2}$	$\frac{3q-2}{4}$	$\frac{3q-2}{4}$

TABLE 1

THE LIGHT CURVE INDEX α AS FUNCTION OF p OR q ($F_{\nu} \propto t^{-\alpha}$). DEFINITION: $\nu_p = \min(\nu_m, \nu_c)$ AND $\nu_0 = \max(\nu_m, \nu_c)$

an afterglow interacts with an outward-expanding fireball, regardless of whether this object is a millisecond magnetar or a Kerr black hole. We find that when the injection energy significantly exceeds the initial energy of the fireball, the bulk Lorentz factor of the wind bubble declines more slowly than before. In addition, the reverse-shock emission could dominate the afterglow emission, which leads to a bump in afterglow light curves. In this paper, we discuss the case of $t_{\text{cr}} < T_{M,0}$. However, even if $t_{\text{cr}} > T_{M,0}$, a bump in Figure 1 still appears for some parameter space as we move the late-time light curve of region 3 to early times.

Bump features have been detected in some events (e.g., GRBs 970508, 000301C, 021004, and 030329). To interpret these features, some other models invoked the microlensing event (Garnavich, Loeb & Stanek 2000), density-jump medium (Dai & Lu 2002; Lazzati et al. 2002; Dai & Wu 2003), pure Poynting-flux injection (Dai & Lu 1998; Zhang & Mészáros 2001), baryon-dominated injection (Rees & Mészáros 1998; Sari & Mészáros 2000; Zhang & Mészáros 2002; Granot, Nakar & Piran 2003), and two-component jet (Berger et al. 2003; Huang et al. 2003). The magnetic field in the reversely-shocked region of the wind bubble seems to consist of two components: a toroidal field and a random field. The latter may be naturally generated by the relativistic two-stream instability (Medvedev & Loeb 1999). If the toroidal field dominates over the random component, one would expect high polarization of the bump emission, which could be used to distinguish between our wind-bubble model and other explanations. It is well known that the degree of linear polarization of synchrotron radiation from the reversely-shocked wind is about $\Pi_{\text{syn}} = (p+1)/(p+7/3)$ for a large-scale toroidal magnetic field. Thus, the polarization of an

afterglow in our model could be as high as $\Pi_{\text{syn}} \sim 70\%$ for $p \sim 2$ when the reverse shock emission dominates the afterglow emission *during an obvious bump*. Even if the total afterglow flux is dominated by the forward shock emission, and the reversely-shocked wind provides only a small fraction of the total flux, ζ , then the shocked pair wind could still dominate the polarized flux with linear polarization of $\Pi \sim \zeta \Pi_{\text{syn}} = 7\%(\zeta/0.1)(\Pi_{\text{syn}}/0.7)$. This value is larger than the currently observed data of GRBs 021004 and 030329 ($\sim 2 - 3\%$, Rol et al. 2003; Lazzati et al. 2003; Greiner et al. 2003). If, on the other hand, the random-field strength exceeds the toroidal component, the calculated degree of linear polarization is significantly less than that estimated above.

We have considered a spherical wind bubble in our paper. However, there is evidence that GRBs are collimated into narrow jets, whose kinetic energy is clustered at $E_{\text{jet}} \sim 10^{50} - 10^{51}$ ergs (Frail et al. 2001; Panaitescu & Kumar 2002; Berger, Kulkarni & Frail 2003; Bloom, Frail & Kulkarni 2003). On the other hand, relativistic winds from millisecond magnetars are roughly isotropic and their total energy is $\sim 10^{53}$ ergs. Beaming correction gives an injection energy of $\sim 10^{51}$ ergs within the initial solid angle of a jet. This energy is of the same order as E_{jet} . Actually, the jet can get more energy from its central magnetar due to sideways expansion. This would favor our model.

The author thanks the referee and B. Zhang for valuable comments and suggestions, and Y. F. Huang, X. Y. Wang, D. M. Wei and X. F. Wu for useful discussions. This work was supported by the National Natural Science Foundation of China (grants 10233010 and 10221001) and the National 973 Project (NKBRSF G19990754).

REFERENCES

Atoyan, A. M. 1999, A&A, 346, L49
 Begelman, M. C., & Li, Z. Y. 1992, ApJ, 397, 187
 Berger, E. et al. 2003, Nature, 426, 154
 Berger, E., Kulkarni, S. R., & Frail, D. A. 2003, ApJ, 590, 379
 Blandford, R., & McKee, C. 1976, Phys. Fluids, 19, 1130
 Bloom, J. S., Frail, D. A., & Kulkarni, S. R. 2003, ApJ, 594, 674
 Chang, H.-Y., Lee, C.-H., & Yi, I. 2002, A&A, 381, L5
 Chevalier, R. A. 2000, ApJ, 539, L45
 Coburn, W., & Boggs, S. E. 2003, Nature, 423, 415
 Coroniti, F. V. 1990, ApJ, 349, 538
 Dai, Z. G., & Lu, T. 1998, Phys. Rev. Lett., 81, 4301
 Dai, Z. G., & Lu, T. 2000, ApJ, 537, 803
 Dai, Z. G., & Lu, T. 2002, ApJ, 565, L87
 Dai, Z. G., & Wu, X. F. 2003, ApJ, 591, L21
 Duncan, R. C., & Thompson, C. 1992, ApJ, 392, L9
 Frail, D. A. et al. 2001, ApJ, 562, L55
 Garnavich, P., Loeb, A., & Stanek, K. 2000, ApJ, 544, L11
 Granot, J., Nakar, E., & Piran, T. 2003, Nature, 426, 138
 Greiner, J. et al. 2003, Nature, 426, 157
 Huang, Y. F., Wu, X. F., Dai, Z. G., Ma, H. T., & Lu, T. 2003, ApJ, in press (astro-ph/0309360)
 Kennel, C. F., & Coroniti, F. V. 1984, ApJ, 283, 694
 Kirk, J. G., & Skjæraasen, O. 2003, ApJ, 591, 366
 Kluźniak, W., & Ruderman, M. 1998, ApJ, 505, L113
 Kumar, P., & Panaitescu, A. 2000, ApJ, 541, L51
 Kumar, P., & Panaitescu, A. 2003, ApJ, submitted (astro-ph/0305446)
 Lazzati, D. et al. 2002, A&A, 396, L5
 Lazzati, D. et al. 2003, A&A, in press (astro-ph/0308540)

Lee, H. K., Wijers, R. A. M. J., & Brown, G. E. 2000, Phys. Rep., 325, 83

Medvedev, M. V., & Loeb, A. 1999, ApJ, 526, 697

Mészáros, P. 2002, ARA&A, 40, 137

Mészáros, P., & Rees, M. J. 1997a, ApJ, 482, L29

Mészáros, P., & Rees, M. J. 1997b, ApJ, 476, 232

Michel, F. C. 1994, ApJ, 431, 397

Narayan, R., Paczyński, B., & Piran, T. 1992, ApJ, 395, L83

Paczynski, B. 1998, ApJ, 494, L45

Panaiteescu, A., & Kumar, P. 2002, ApJ, 571, 779

Rees, M. J., & Gunn, J. E. 1974, MNRAS, 167, 1

Rees, M. J., & Mészáros, P. 1998, ApJ, 496, L1

Rees, M. J., & Mészáros, P. 2000, ApJ, 545, L73

Rol, E. et al. 2003, A&A, in press (astro-ph/0305227)

Ruderman, M. A., Tao, L., & Kluźniak, W. 2000, ApJ, 542, 243

Sari, R., & Mészáros, P. 2000, ApJ, 535, L33

Sari, R., & Piran, T. 1999, ApJ, 517, L109

Sari, R., Piran, T., & Narayan, R. 1998, ApJ, 497, L17

Spruit, H. C. 1999, A&A, 341, L1

Usov, V. V. 1992, Nature, 357, 472

Wheeler, J. C., Yi, I., Höflich, P., & Wang, L. 2000, ApJ, 537, 810

Woosley, S. E. 1993, ApJ, 405, 273

Zhang, B., & Mészáros, P. 2001, ApJ, 552, L35

Zhang, B., & Mészáros, P. 2002, ApJ, 566, 712

Zhang, B., Kobayashi, S., & Mészáros, P. 2003, ApJ, 595, 950

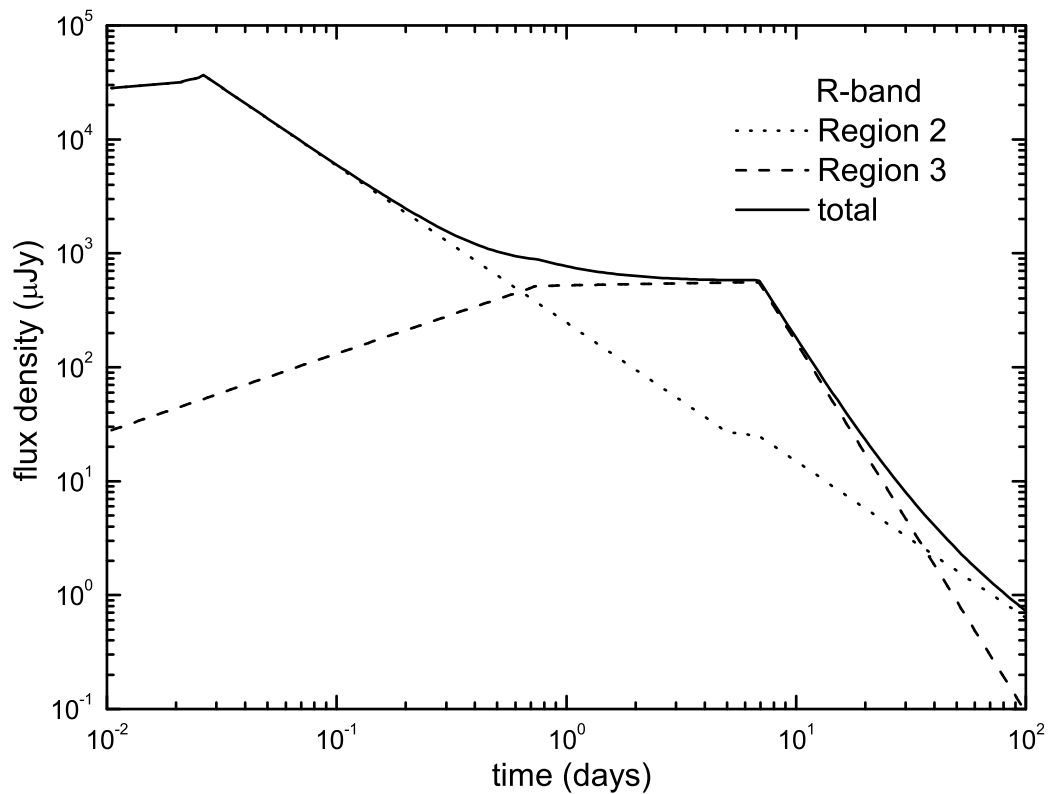


FIG. 1.— R-band light curves of the emissions from regions 2 (dotted line) and 3 (dashed line). The solid line corresponds to the total flux.